M&MS

A NOVEL DEEP PENETRATING EDDY CURRENT PROBE BASED ON PHASE SHIFTED FIELDS AND ITS APPLICATION TO INSPECTION OF DEFECTS

Meixian Wu, Dongli Zhang, Chuanglong Wang

North Minzu University, School of Chemistry and Chemical Engineering, 204 North Wenchang Road Xixia District, 750021, Yinchuan, Ningxia, China (1312377989@qq.com, ✉ zdlsir@163.com, +86 184 0867 1551, 1776040014@qq.com)

Abstract

Due to the skin effect of eddy currents, the depth of cracks which can be detected by the traditional eddy current probe is very limited. In order to improve the ability of eddy current probes to inspect deep cracks in metal thick-walled structures, a new eddy current probe using an excitation system with phase shifted fields was proposed. Its feasibility for detecting deep cracks was verified by simulation and experiments. The results showed that the penetration depth of eddy currents in austenitic stainless steel is effectively enhanced by using the new probe.

Keywords: skin effect, penetration depth, austenitic stainless steel, eddy current probe, phase shifted fields.

1. Introduction

Nondestructive testing (NDT) methods are widely used in petrochemical, metallurgical power, aerospace, nuclear power and other important fields. It is of great significance to ensure the safety of equipment operation and reduce the cost of maintenance and, especially, to quantitatively evaluate the hidden defects or deep cracks developing in some large key components, which will cause serious consequences such as major accidents in the future.

The common detection methods of internal defects or deep cracks include the *radiographic testing* method (RT), the *ultrasonic testing* method (UT) and the *alternating current potential drop* method (ACPD) [1–6], *etc*. But limited by the working mechanism, they are not suitable for fast quantitative on-line detection of large components. For example, it is very difficult by using the RT technique to find defects parallel to the material surface. And it is also impossible to complete the detection of large work-pieces by using the UT method in a short time because the coupling agent is required during its operation. While the ACPD method is only applicable to inspection of surface-breaking cracks.

The *eddy current testing* method (ECT) is an effective method for evaluation of sub-surface defects quantitatively. It has the advantages of non-contact, fast speed and quantitative analysis of

shallow cracks. Due to the skin effect, eddy currents are limited to the surface and near surface of the conductor at high frequency. To overcome the difficulty, scholars have tried many ways to increase the penetration depth of eddy currents for inspection of deep cracks. One of the typical methods applied is the *low-frequency eddy current* testing technology (LFET) [7, 8]. The penetration depth can be enhanced, but low resolution, low signal-to-noise ratio and low detection speed at the same time are obvious disadvantages of this method. In recent years, some new ideas have emerged [9–13]. Janousek [14] proposed a new type of the eddy current probe. The point is, however, that the eddy currents induced in metal materials by the new probe have directionality, which can leave some defects undetected. This shortcoming seriously limits its application range.

In the paper, a new deep penetrating probe with coils of pancake type is proposed. It is not sensitive to the direction of cracks and has the ability of detecting deep cracks.

2. Working principle of the new probe

Due to the limit of the skin effect, it is very difficult to induce deep penetrating eddy currents in conductive materials with a conventional probe. To attenuate the skin effect, the new probe proposed in the paper uses two circular coils of different sizes as the excitation source to induce deep penetrating eddy currents in the material. The deep penetrating currents are the superposition results of eddy currents induced by the two coils respectively. The new distribution has zero value on the material surface and non zero value in the material along depth, which is beneficial for detecting deep defects.

Assuming there are two coils fed with the applied current density respectively

$$i_1 = i'_1 e^{j\omega t} \quad \text{and} \quad i_2 = i'_2 e^{j\omega t}, \tag{1}$$

where ω is the circular frequency. i'_1 and i'_2 are the amplitudes of i_1 and i_2.

According to reference [15], the eddy current density induced at point (x, z) in the conductive material (Fig. 1a) can be calculated by using the following formulas

$$J(x_1, z) = -j\omega\sigma A_1(x_1, z), \tag{2}$$

$$J(x_2, z) = -j\omega\sigma A_2(x_2, z), \tag{3}$$

where $J(x_1, z)$ and $J(x_2, z)$ are the densities of eddy currents induced by the inputs i_1 and i_2. σ is the material conductivity. The vector potentials A_1 and A_2 are determined by

$$
\begin{aligned}
A_1(x_1, z) = \mu i_1 \int_0^\infty (1/\alpha^3) I_1(r_{o1}, r_{i1}) J_1(\alpha x_1) \left[\exp(-\alpha l_1) - \exp(-\alpha l_2)\right] \\
\times \left[\frac{\alpha(\alpha_2 + \alpha_1)\exp(2\alpha_1 c)\exp(\alpha_1 z) + \alpha(\alpha_1 - \alpha_2)\exp(-\alpha_1 z)}{(\alpha - \alpha_1)(\alpha_1 - \alpha_2) + (\alpha + \alpha_1)(\alpha_2 + \alpha_1)\exp(2\alpha_1 c)} \right] d\alpha
\end{aligned}
\tag{4}
$$

$$
\begin{aligned}
A_2(x_2, z) = \mu i_2 \int_0^\infty (1/\alpha^3) I_2(r_{o2}, r_{i2}) J_1(\alpha x_2)[\exp(-\alpha l_1) - \exp(-\alpha l_2)] \\
\times \left[\frac{\alpha(\alpha_2 + \alpha_1)\exp(2\alpha_1 c)\exp(\alpha_1 z) + \alpha(\alpha_1 - \alpha_2)\exp(-\alpha_1 z)}{(\alpha - \alpha_1)(\alpha_1 - \alpha_2) + (\alpha + \alpha_1)(\alpha_2 + \alpha_1)\exp(2\alpha_1 c)} \right] d\alpha
\end{aligned}
\tag{5}
$$

with I_1 and I_2, the integral results of J_1, given respectively by

$$\int_{r=r_{i1}}^{r_{o1}} r J_1(\alpha r)\, dr \equiv (1/\alpha^2) I_1(r_{o1}, r_{i1}), \tag{6}$$

$$\int_{r=r_{i2}}^{r_{o2}} r J_1(\alpha r)\, dr \equiv (1/\alpha^2) I_2(r_{o2}, r_{i2}) \tag{7}$$

and the separation constants α and α_i defined by

$$[1/Z(z)]\partial^2 Z(z)/\partial z^2 = \alpha^2 + j\omega\mu\sigma_i, \tag{8}$$

$$\alpha_i \equiv (\alpha^2 + j\omega\mu\sigma_i)^{1/2}, \tag{9}$$

where l_1 is the coil lift-off. $l_2 - l_1$ is the coil thickness. The parameters r_{i1} and r_{o1} are the inner and outer radii of Coil 1 respectively. r_{i2} and r_{o2} are those of Coil 2. J_1 is a Bessel function of the first order. The parameters μ and c are the permeability and thickness of the material respectively.

When the two excitation coils are fed with input currents of opposite direction, the superposition result of eddy current density in the material is

$$J(x_1, z) - J(x_2, z) = -j\omega\sigma A_1(x_1, z) + j\omega\sigma A_2(x_2, z). \tag{10}$$

Adjusting the input currents of the two coils can make the eddy current density on the material surface at the picking-up position become zero, that is to say:

$$J(x_1, 0) - J(x_2, 0) = 0. \tag{11}$$

Then, a new distribution of eddy currents will be obtained as shown in Fig. 1b.

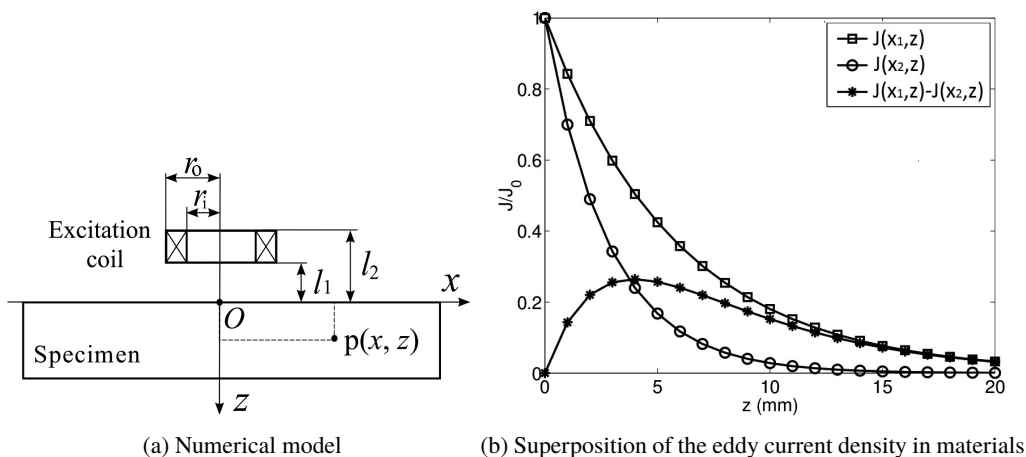(a) Numerical model   (b) Superposition of the eddy current density in materials

Fig. 1. Generation of the new distribution of eddy currents.

The superposition effect depends on the curve shape of eddy current density. The greater the shape difference between the two curves, the deeper the concentration position of superposed eddy currents and the stronger the ability of the probe for inspection of deep cracks. The shape of the curves depends on the size and position of the two excitation coils as well as the excitation frequency. By adjusting these parameters, the superposition effect can be optimized.

3. Influencing factors of penetration

In order to achieve a high performance of the new probe, the main factors affecting the curve shape of eddy current density and the *standard depth of penetration* (SDOP) are analyzed by simulation, including the radius of the excitation coil, the coil lift-off, the picking-up position and the core material. Ordinarily, the eddy current density remains greatest at the material surface and decreases with increase of depth. SDOP, the penetration capability index of eddy currents, is defined as the depth at which the eddy current density is 37% of the value at the surface of the material. However, for the new eddy current probe proposed in the paper, the maximum density of eddy currents induced in the material is not on the material surface. The definition of SDOP is revised to the depth at which the eddy current density becomes 37% of the maximum value.

For the sake of simplicity, firstly, one excitation coil is modeled to analyze the factors affecting the penetration depth of eddy currents in this section. Then based on the conclusions of Section 3, two excitation coils are configured to obtain the best penetration depth in the material in Section 4. Because only the distribution of eddy currents generated by the excitation coil is analyzed, an excitation coil and a specimen made of 304 austenitic stainless steel are considered in the numerical modelling (Fig. 2). The default outer radius, inner radius and height of the coil used for analysis are $r_o = 1.6$ mm, $r_i = 0.6$ mm and $h_c = 0.8$ mm, respectively. The excitation current and frequency are 1 A and 1 kHz respectively. The coil lift-off is 0.5 mm. The specimen is 100 mm long, 100 mm wide and 25 mm thick.
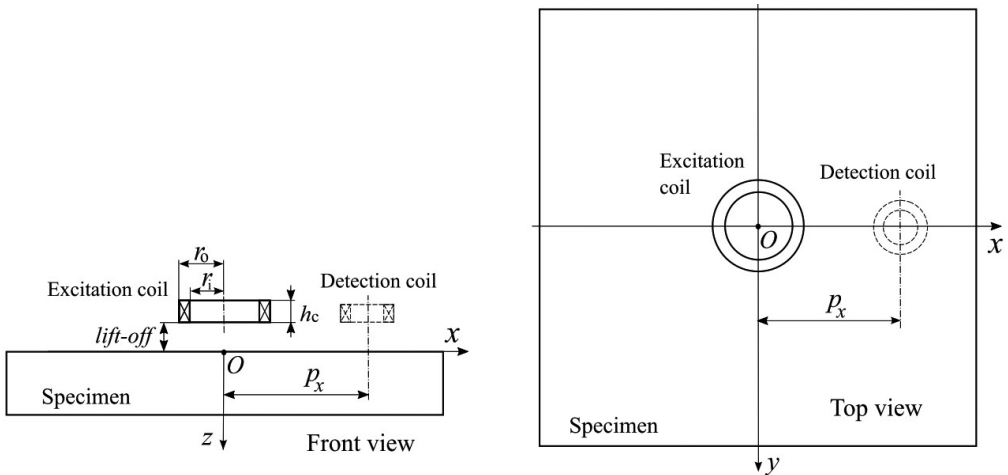

Fig. 2. The numerical model for analysis of penetration.

3.1. Radius of the excitation coil

Coil radius is one important factor that affects penetration depth. The simulation results are normalised according to the eddy current density on the surface of the material. If the eddy current density is normalized by using its surface value, we can easily obtain the SDOP value which corresponds to the normalized value 0.37. Figure 3 shows the normalised results for the coil outer radius r_o increasing from 1.6 mm to 16 mm with increments of 3.2 mm, whereas the differences between outer and inner radii remain constant at 1 mm. The coil height h_c is 0.8 mm.
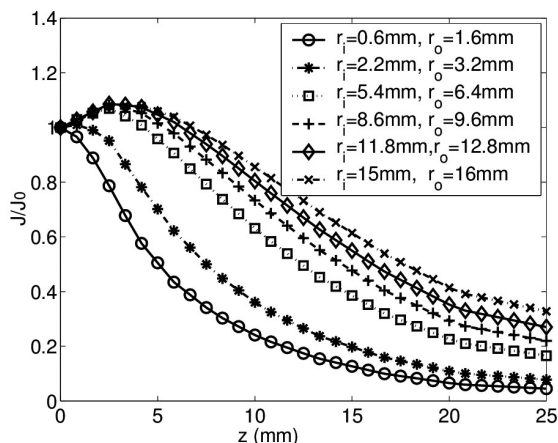
Fig. 3. The relation between coil radius and eddy current distribution.

The results show that the coil radius has a significant effect on the distribution and further the penetration depth. With the increase in coil radius, the penetration depth as well as the shape difference in eddy current distribution curve increases obviously. The results from Table 1 show that when the coil radius changes from 3.2 mm to more than 6.4 mm, the SDOP increases to about 2 times of the original value.

The ideal distribution is that the eddy currents superimposed on the surface of the material are zero. It can be expected that if there is a large difference between the coil radii, a new distribution of deep penetration can be obtained by superposition of the eddy currents in the opposite direction. The bigger the difference in coil radii, the bigger the penetration depth after superposition.

Table 1. The relation between coil radius and SDOP.

r_o [mm]	1.6	3.2	6.4	9.6	12.8	16
SDOP [mm]	6.99	9.81	15.39	17.69	19.51	22.23

3.2. Picking-up position

The defect depth that can be detected by the eddy current probe depends not only on the excitation frequency, but also on the position of the detection coil. Figure 4 shows the ratio of the eddy current density inside the material to that on the material surface at different locations, which is the result by using a coil of default dimension. The x axis is the position of the measuring point, that is, the distance between the detecting coil and the exciting coil. $X = 0$ means that the measuring point is located at the center of the excitation coil. The y axis is the relative value of eddy current density. The figure presents the distribution of eddy currents along the radial direction of the excitation coil at different depths of the material. The bigger the y value is, the bigger the eddy current density inside the material is relative to that on the material surface. For example, the y value of the curve "$z = 16.6$ mm" at $x = 0$ is about 0.1, which is smaller than the value $y = 0.37$ corresponding to the standard penetration depth. This means that when the detection coil is located at $x = 0$, the defect at the

depth of 16.6 mm in the material is not easy to detect. Only when the distance between the excitation coil and the detection coil increases to 10 mm, the defect of 16.6 mm depth can be detected.
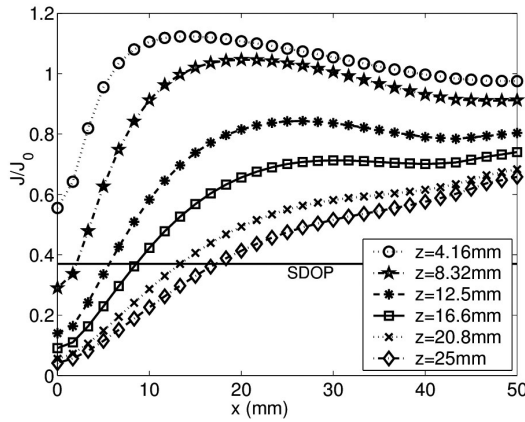

Fig. 4. Eddy current distributions along radial direction at different depths.

From these results, it can be seen that the depth of defects that can be detected depends on the distance between the excitation coil and the detection coil. The larger the distance, the deeper defect can be detected. For the two excitation coils working simultaneously, if the distance between the two excitation coils and the detection one is different, a larger penetration depth can be achieved after the superposition of eddy currents. In order to ensure the detection signals to be big enough, the distance between the excitation coil and the detection coil should not be too big.

3.3. Lift-off of excitation coil

The results in Fig. 5a are the lift-off effect for a small excitation coil with dimensions of $r_o = 1.6$ mm, $r_i = 0.6$ mm and $h_c = 0.8$ mm. The eddy current density is obtained at the point

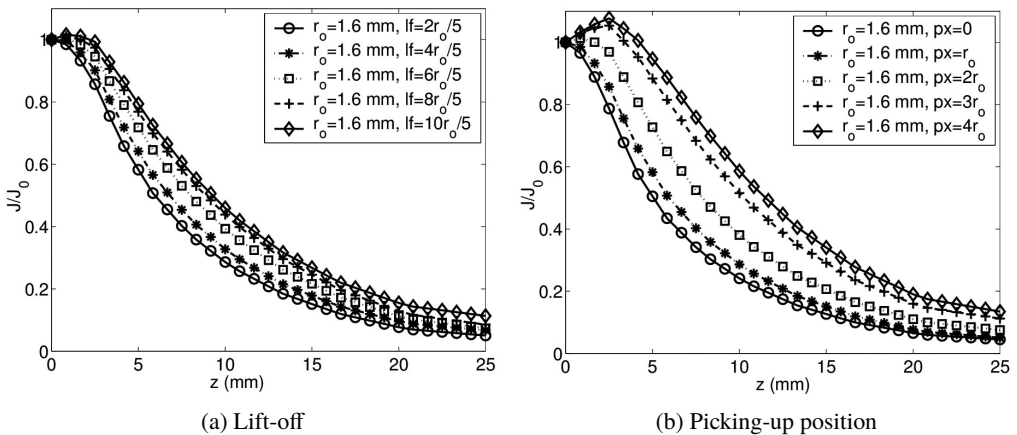
(a) Lift-off   (b) Picking-up position

Fig. 5. The relation between lift-off, picking-up position and eddy current distribution.

$p_x = (r_i + r_o)/2$. It shows that the SDOP of eddy currents increases with the lift-off from $2r_o/5$ to $2r_o$. The effect is small for the excitation coil of a small radius. Figure 5b shows the comparison of the lift-off effect at different picking-up positions when the lift-off is set as $lf = 2r_o/5$. From the results it can be seen that the lift-off effect of the excitation coil depends not only on the coil size, but also on the position of the detection coil.

3.4. Core material of excitation coil

Ferrite cores are often applied to eddy current probes to improve resolution and reduce the size of the probe. Figure 6a shows a comparison of eddy current distributions driven by an air-core probe and a solid ferrite-core probe with the coil of default dimension at different frequencies respectively. The results are all obtained at $p_x = (r_i + r_o)/2$. The material of the core is MnZn with resistivity of 4 Ωm and relative permeability of 2500. The results show that in comparison with the air-core probe, though the ferrite-core probe can obtain better magnetic coupling and induce stronger eddy currents, its contribution to penetration is the same as in the case of the air-core type.

Figure 6b shows the results for the excitation coil with a ring ferrite-core. The outer radius r_{oc} of the core is the same as the inner radius r_i of the coil, and the inner radius r_{ic} of the core varies from 0 to $r_{oc}/2$. The core with $r_{ic} = 0$ represents a solid one. The results show that the penetration depth of eddy currents increases with the increase of r_{ic}. For r_{ic} being half of r_{oc}, the penetration depth reaches the maximum. It shows that, in comparison with the solid core, the ring core can make a contribution to improvement of the penetration depth.
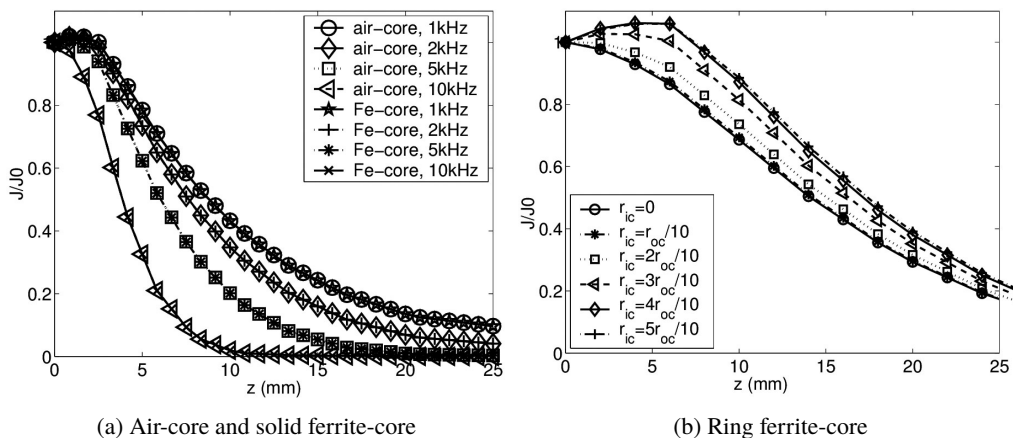

(a) Air-core and solid ferrite-core   (b) Ring ferrite-core

Fig. 6. Comparison of eddy current distributions induced by coils with air-core and ferrite-core.

4. Configuration of the new probe

Based on the analysis above, a new deep penetrating probe is designed. As shown in Fig. 7, two exciting coils of different sizes are selected to form the excitation part of the new probe. Deep penetration of eddy currents is realized by superposition of two eddy currents in opposite

directions. In order to reduce the probe size, Coil 2 is placed under Coil 1, and Coil 3, the pick-up coil is placed beside Coil 2. In order to avoid the influence of the exciting magnetic field on the detecting coil and obtain high detection sensitivity, a magnetic shield is mounted on the pick-up coil.
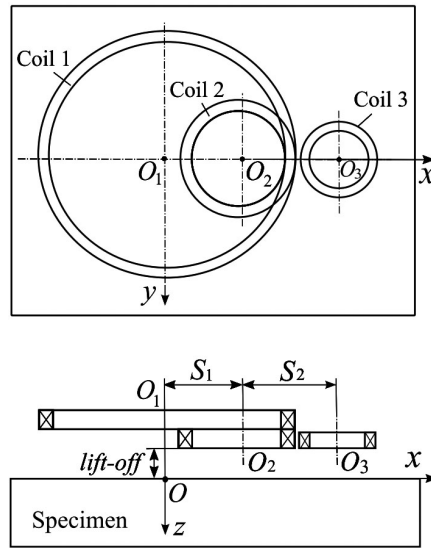

Fig. 7. Configuration of the new probe.

To make the eddy currents superimposed on the material surface become zero, the magnitude and phase of input currents of Coil 1 and Coil 2 are adjusted as follows according to the amplitude and phase of eddy currents induced on the material surface:

First, the amplitude ratio $k = J(x_1, 0)/J(x_2, 0)$ and phase difference $\Delta\varphi = \varphi_1 - \varphi_2$ between the eddy current densities on the material surface are obtained through simulation for Coil 1 and Coil 2 excited respectively by the input currents $i_1 = i_2 = \sqrt{2}I_1 \sin(2\pi ft)$. Second, to make the eddy currents induced by the two coils flowing in the opposite direction on the material surface equivalent, the amplitude and phase of the exciting currents in Coil 2 are adjusted to $I_2 = kI_1$ and $\varphi_2 = \Delta\varphi + \pi$, respectively. Then, the superposition result of eddy currents on the material surface will become zero.

The distance between the coils is one important factor affecting the penetration depth. As shown in Fig. 7, S_1 and S_2 are the distances between the centers of coils 1 and 2, 2 and 3, respectively. Simulation results show that when $S_1 = r_{O1} - r_{O2}$ and $S_2 = 2r_{O2}$, the largest penetration depth could be obtained. Figure 8 compares the eddy current distribution obtained by the new probe with that obtained by a traditional probe at the frequency of 1 kHz. Tables 2 and 3 show their coil parameters. The numbers presented in Fig. 8 are the values of SDOP and the corresponding normalized eddy current density. They are obtained according to the revised definition of SDOP, that is, the depth at which the eddy current density becomes 37% of the maximum value. It can be seen that when the probes are excited at 1 kHz, the penetration depth brought by the new probe can reach 26.3 mm, while that brought by the traditional one only can reach 11.2 mm.
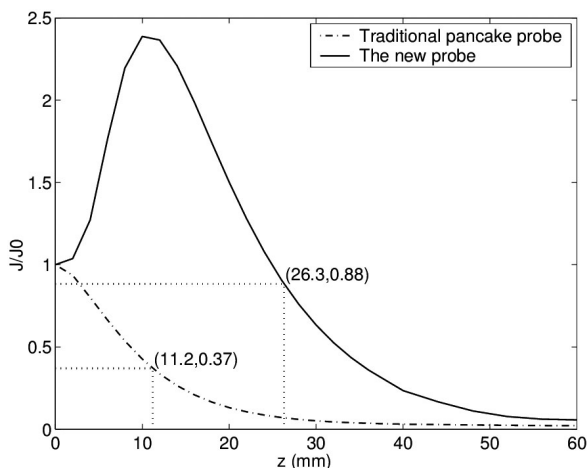
Fig. 8. Performance comparison between the new probe and a traditional one.

Table 2. Coil parameters of the new probe.

	r_o [mm]	r_i [mm]	h_c [mm]	1 kHz	
				I [A]	φ [°]
Coil 1	16 mm	14 mm	1.6 mm	1	0
Coil 2	3.2 mm	1.2 mm	1.6 mm	7.5	167
Coil 3	1.6 mm	0.6 mm	0.8 mm		

Table 3. Coil parameters of the traditional probe.

r_o [mm]	r_i [mm]	h_c [mm]	I [A]	f [kHz]
16 mm	14 mm	1.6 mm	1 A	1

5. Application of the new probe to inspection of deep cracks

5.1. Simulation results

In order to verify the performance of the new probe, the detection signals of cracks at different depth by using the new probe and a traditional one are simulated and compared. The detection signals of two types of defects (Fig. 9) are simulated, including inner defects (ID) and outer defects (OD). They are set on a SUS304 stainless steel specimen with the size of $1350 \times 175 \times 30$ mm^3. The width w_d and length l_d of these defects are set at 0.2 mm and 175 mm respectively. The sensitivity of the probe to the change of defect depth h_d was also compared. For OD, h_d denotes the distance between the defect tip and the material surface.

Figure 10 show the simulation results of the impedance signals for h_d changing from 2 mm to 26 mm at the frequency of 5 kHz. From the results, it can be seen that, regardless of the defects being ID or OD, the new probe is more sensitive to the change of defect depth than the traditional one.
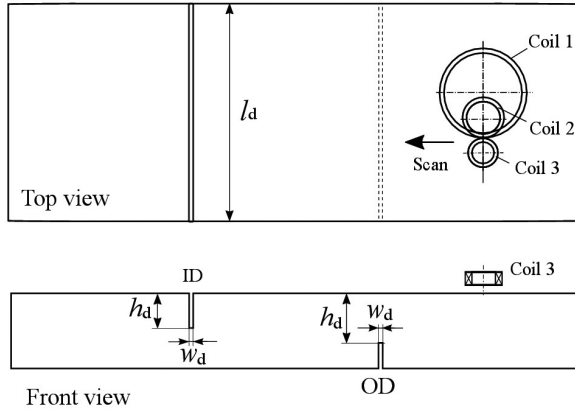
283

Fig. 9. The defects models.

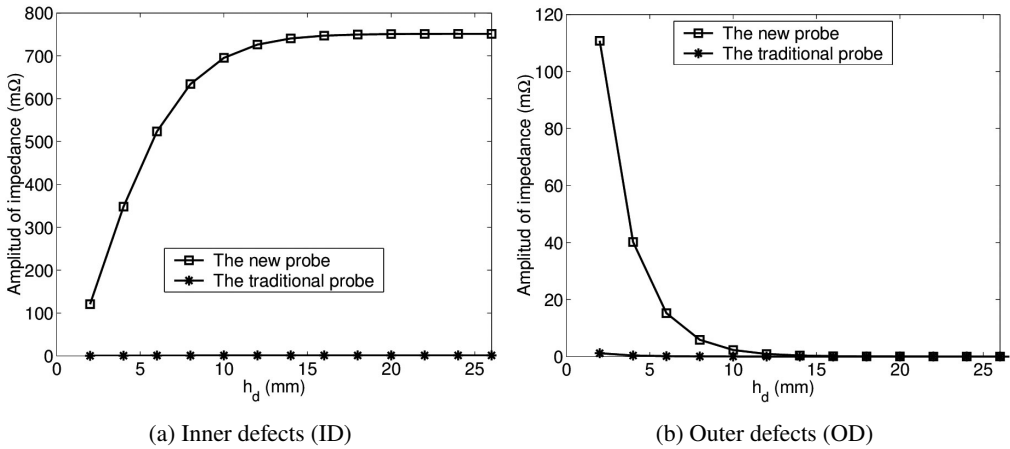(a) Inner defects (ID)

(b) Outer defects (OD)

Fig. 10. Comparison of detection signals between the new probe and a traditional one.

Table 4 shows the sensitivity of the probe to ID depth change, *i.e.* the variation of impedance Δz for every 2 mm increase in crack depth h_d. It is calculated according to the formula below:

$$\Delta z_1(h_{d,i}) = z\left(h_{d,(i+1)}\right) - z(h_{d,i}), \quad \text{for the new probe,} \tag{12}$$

$$\Delta z_0(h_{d,i}) = z\left(h_{d,(i+1)}\right) - z(h_{d,i}), \quad \text{for the traditional probe.} \tag{13}$$

where, $\Delta z_1(h_{d,i})$ is the amplitude change of impedance with the new probe to detect the crack of depth of $h_{d,i}$ and $h_{d,(i+1)}$. $\Delta z_0(h_{d,i})$ is that with the traditional probe. $\Delta z_1/\Delta z_0$ is the ratio of crack detection signal variation at different depths obtained by using two probes.

It can be seen that, comparing with the traditional probe, the new one is more sensitive to ID depth change. The impedance change of the new probe is bigger than that of the traditional one.

PAN

Metrol. Meas. Syst., Vol. 27 (2020), No. 2, pp. 275–287

DOI: 10.24425/mms.2020.132774

POLSKA AKADEMIA NAUK

Table 4. Comparison of sensitivity to crack depth between the new probe and a traditional one.

$h_{d,i}$ [mm]	2	4	6	8	10	12	14	16	18	20	22	24
Δz_1 [mW]	227.4	175.6	110.3	61.1	30.9	14.5	6.4	2.6	1.0	0.38	0.13	0.04
Δz_0 [mW]	391.1	234.9	124.3	61.4	28.9	13.1	5.7	2.4	0.96	0.37	0.14	0.05
$\Delta z_1/\Delta z_0$	581	747	887	994	1067	1109	1124	1114	1083	1036	978	920

5.2. Experimental verification

To verify the conclusions, the new probe is designed and made for inspection of real cracks. As shown in Fig. 11. the excitation coils and the detection coil are wound on three wrapping posts with enameled wire respectively. Coil 2 is placed in a guide slot to adjust the distance between Coil 2 and Coil 1. They are all fixed on a rectangular framework. The two coils both have 35 turns and the wire diameter used for them is 0.3 mm.

The experimental system is shown in Fig. 12. Two bipolar power supplies are used to provide excitation signals at 5 kHz for Coil 1 and Coil 2, respectively. The input currents are 2 A and 0.18 A respectively with phase difference of 102 degrees. The crack signals are picked up by Coil 3 and transferred to the oscilloscope.
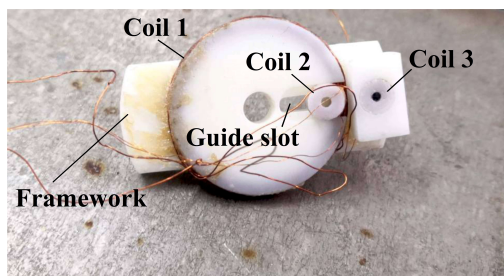

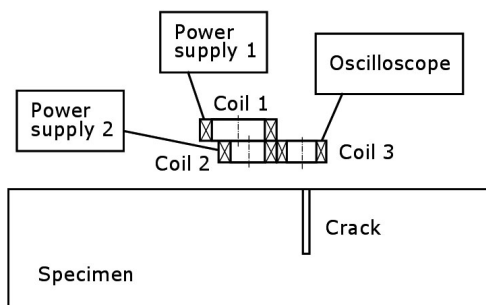Fig. 11. The new eddy current probe.

Fig. 12. The eddy current inspection system.

There are three SUS304 stainless steel specimens of same size $1350 \times 175 \times 20$ mm^3 machined as shown in Fig. 13. Several through grooves with 1 mm width and depth ranging from 3 mm to 15 mm are machined on them.

The simulation shows that signal differences for ODs are smaller than those for IDs. This means that it is not easy to distinguish the OD depth by signal differences. To overcome the difficulty, a large-scale detection coil (with outer radius $r_o = 10$ mm, inner radius $r_i = 8$ mm and height $h = 10$ mm) is used to pick up the OD signal, whereas the ID signal is obtained by using Coil 3 listed in Table 2 (with $r_o = 1.6$ mm, $r_i = 0.6$ mm and $h = 0.8$ mm).

Fig. 14 presents the experimental results for both IDs and ODs. The results show that the amplitudes of detection signals for cracks at different depths are different. The depth of the crack can be identified by the amplitude of the disturbance signal. IDs are easier to detect than ODs. An ID at a depth of 15 mm is easy to detect, while an OD can be detected at the depth of no more than 8 mm.
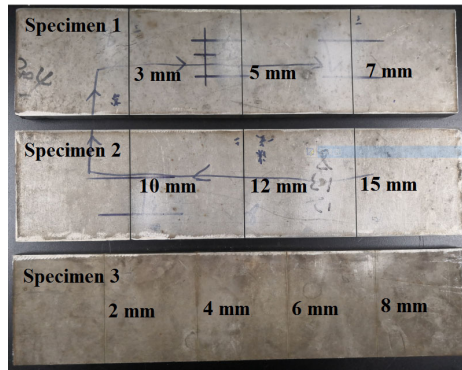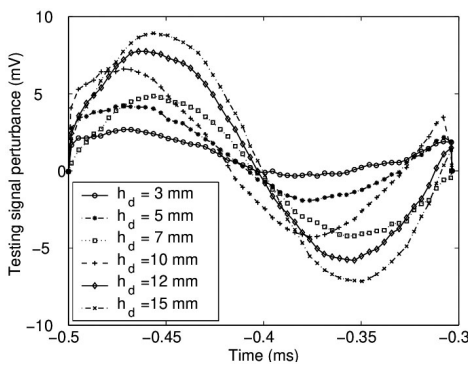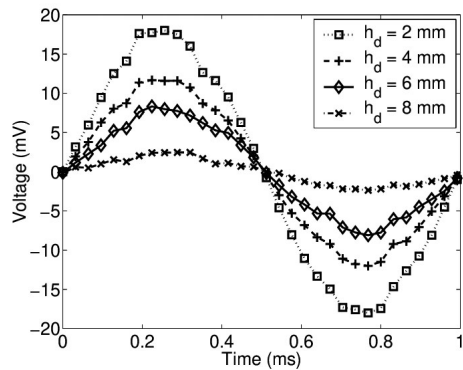
285

Fig. 13. Specimens.

(a) ID Specimens 1 and 2   (b) OD Specimens 3

Fig. 14. Experimental results.

6. Conclusions

In this paper, the main factors affecting the penetration depth of eddy currents were analyzed. It is found that the penetration can be enhanced greatly by optimizing these parameters. Based on the conclusion, a new type of eddy current probe for inspection of deep cracks and hidden defects in materials was proposed. The probe uses two coils of pancake type to generate eddy currents of large penetration depth in stainless steel through adjustment of input currents and configuration of excitation coils. Compared with the traditional probe, the new one is more sensitive to the change of depth of the defect. Using the maximum value of eddy current density as reference to calculate the standard penetration depth, for the new probe driven at 1 kHz or 5 kHz, the penetration depth in SUS304 can exceed 15 mm. Simulation and experimental results confirm its performance for detecting deep defects quantitatively.

Acknowledgements

References

[1] Eason, G., Noble, B. Sneddon, I.N. (1955). On certain integrals of Lipschitz-Hankel type involving products of Bessel functions. *Philosophical Transactions of the Royal Society of London*, 247(935), 529–551.

[2] Baniukiewicz, P. (2014). Automated Defect Recognition and Identification in Digital Radiography, *Journal of Nondestructive Evaluation*, 33, 327–334.

[3] Zapata, J., Vilar, R., Ruiz, R. (2011). Performance evaluation of an automatic inspection system of weld defects in radiographic images based on neuro-classifiers. *Expert Systems with Applications*, 38(4), 8812–8824.

[4] Martín, Ó., Pereda, M., Santos, J.I., Galán, J.M. (2014). Assessment of resistance spot welding quality based on ultrasonic testing and tree-based techniques. *Journal of Materials Processing Technology*, 214(8), 2478–2487.

[5] Chakrapani, S.K., Padiyar, M.J., Balasubramaniam, K. (2012). Crack detection in full size Cz-silicon wafers using lamb wave air coupled ultrasonic testing (LAC-UT). *Journal of Nondestructive Evaluation*, 31(1), 46–55.

[6] Yeh, C.P., Huang, J.Y. (2018). Numerical simulations of electric potential field for alternating current potential drop associated with surface cracks in low-alloy steel nuclear material. *Nondestructive Testing and Evaluation*, 33(1), 175–188.

[7] Raja, M.K., Mahadevan, S., Rao, B.P.C., Behera, S.P., Jayakumar, T., Raj, B. (2010). Influence of crack length on crack depth measurement by an alternating current potential drop technique. *Measurement Science and Technology*, 21(7), 105702.

[8] Alatawneh, N., Underhill, P.R., Krause, T.W. (2017). Low-frequency eddy-current testing for detection of subsurface cracks in CF-188 stub flange. *IEEE Sensors Journal*, 18(4), 1568–1575.

[9] Weimin, L., Changyu, S., Zhouhong, Z., Zexu, L., Fengying, S., Weixin, X., *et al*. (2018). Internal defect detection in ferromagnetic material equipment based on low-frequency electromagnetic technique in 20# steel plate. *IEEE Sensors Journal*, 18(16), 6540–6546.

[10] Kawano, J., Hato, T., Adachi, S., Oshikubo, Y., Tsukamoto, A., Tanabe, K. (2010). Non-destructive evaluation of deep-lying defects in multilayer conductors using HTS SQUID gradiometer. *IEEE Transactions on Applied Superconductivity*, 21(2), 428–431.

[11] Sakthivel, M., George, B., Sivaprakasam, M. (2015). A novel GMR-based eddy current sensing probe with extended sensing range. *IEEE Transactions on Magnetics*, 52(4).

[12] Cheng, W., Komura, I. (2010). Optimum inducement of eddy current for NDE of deep lying defects: An analytical approach. *International Journal of Applied Electromagnetics and Mechanics*, 33(1–2), 377–385.

[13] Zuo, Y., Chen, Z., Mao, Y., Zhang, J. (2010). Enhancement of sizing capability of ECT for deep cracks by using split TR probes. *International Journal of Applied Electromagnetics and Mechanics*, 33(3–4), 1157–1164.

[14] Janousek, L., Chen, Z., Yusa, N., Miya, K. (2005). Excitation with phase shifted fields-enhancing evaluation of deep cracks in eddy-current testing. *NDT&E International*, 38(3), 508–515.

[15] Dodd, C.V., Deeds, W.E. (1968). Analytical solutions to eddy-current probe-coil problems. *Journal of Applied Physics*, 39(3), 2829–2838.